Effect of Polydispersity on the Phase Diagrams of Linear ABC Triblock Copolymers in Two Dimensions

Ying Jiang,[†,‡] Xiaoyan Yan,[†,‡] Haojun Liang,*[,†,‡] and An-Chang Shi[§]

Hefei National Laboratory for Physical Sciences at Microscale, University of Science and Technology of China, Hefei, Anhui 230026, People's Republic of China, Department of Polymer Science and Engineering, University of Science and Technology of China, Hefei, Anhui 230026, People's Republic of China, and Department of Physics and Astronomy, McMaster University, Hamilton, Ontario L8S4M1, Canada

Received: June 1, 2005; In Final Form: September 8, 2005

By using a two-dimensional (2D) real-space self-consistent field theory, we present the phase diagrams of monodisperse ABC triblock copolymers in a three-component triangle style with the interaction energies given between the distinct blocks; this system displays richer phase behavior when compared with the corresponding diblock copolymers. Polydispersity of the end or middle blocks in the ABC linear block copolymer chains results in a completely different phase diagram. The presence of a polydisperse end block may cause strong segregation to occur among the three distinct components and larger domain sizes of the dispersed phases; a polydisperse middle block may allow a connection to form between the two phases of the two end blocks.

1. Introduction

Block copolymers are formed by chemically linking different polymer chains together. Because of the repulsive interactions between the different blocks and the topological constraints caused by the subchains being linked permanently, block copolymers can self-assemble to form a variety of ordered structures in melts and concentrated solutions. The self-assembled structures that block copolymers form have fascinated researchers from both theoretical and applied perspectives for four decades.[1] For the simplest case of an AB diblock copolymer, the thermodynamic balance between the segment−segment interaction energy (χ) and the chain-stretching-driven changes in entropy causes block copolymers to microphase separate into well-ordered structures below an order−disorder transition determined by the product χN, where N is the degree of polymerization. Four stable ordered structures have been documented for monodisperse AB diblock copolymers:[2−4] lamellae, gyroids, cylinders, and spheres. Recently, Tyler and Morse predicted theoretically a fifth stable structure, O^{70}, that exists within a narrow, very weakly segregated region and competes closely with the gyroid phase; this state has not been observed experimentally because of fluctuation effects.[5] In the last few decades, a great deal of experimental and theoretical effort has been spent on the study of diblock copolymers; the phase behaviors of these simple systems are now well understood.

Although diblock copolymers provide a rich phase behavior and five ordered phases, it remains desirable to search for the possibility of producing more varied phases from block copolymers. This search can be studied in two ways. The first is through blending, in which different block copolymers and homopolymers are mixed to produce ordered phases.[6−16] The other is to enlarge the number of monomers present in the block copolymers. The simplest approach in this latter direction is to study ABC triblock copolymer systems. Relative to their corresponding AB diblock copolymers, significant increases occur in both the complexity and variety of structures self-assembled from ABC triblock copolymers, i.e., upon increasing the number of distinct blocks from two to three.[17−20] First of all, the number of controlling parameters increases from two to five, leading to a huge phase space to be explored. Furthermore, for triblock copolymers, the microphases depend not only on the composition and interaction energies between the distinct blocks, but also on their particular molecular architectures, i.e., whether the sequence of the blocks in the chain follows the order A−B−C, B−C−A, or C−A−B.[21−24]

Because of their rich phase behaviors, ABC triblock copolymers have attracted a great deal of attention from theoreticians. Among the different theoretical tools, the self-consistent field theory (SCFT) provides a powerful technique for studying the phases and phase transitions of polymeric systems. SCFT is a mesoscopic simulation technique formulated by Edwards in the 1960s and adapted by Helfand and others explicitly for the study of block copolymers. This technique has been extremely useful for studies of inhomogeneous polymers and complex fluid phases.[25−31] The application of such methods to dense phases, including melts and concentrated solutions of homo, block, and graft copolymers, has been particularly fruitful for unraveling the complexities of their self-assembled structures at equilibrium. Matsen and Schick[27] have solved the SCFT equation successfully by using a "spectral" approach; this method is numerically efficient and allows high-precision calculations of free energies and phase diagrams to be made, but it has the flaw that the relevant morphologies must be known a priori. To circumvent this problem, Drolet and Fredrickson recently suggested the implementation of SCFT for monodisperse block copolymers, where low free-energy morphologies are found through relaxation from random potential fields.[29−31] A similar real-space approach has also been suggested by Bohbot-Raviv and Wang.[32]

In most of these theoretical approaches, it is assumed that the polymers are monodisperse, but most, if not all, synthetic

* Corresponding author. E-mail: hjliang@ustc.edu.cn.
† Hefei National Laboratory for Physical Sciences at Microscale.
‡ Department of Polymer Science and Engineering.
§ Department of Physics and Astronomy, McMaster University.

10.1021/jp052902y CCC: $30.25
Published on Web 10/13/2005

polymers are polydisperse. It is well-known that many of the unique static and dynamic properties of polymers depend on their chain lengths,[1] and it is expected that a larger polydispersity will influence those properties. For example, the effect that polydispersity has on the relaxation of concentration fluctuations in diblock melts and solutions has been investigated.[33] There have been a few theoretical studies in which polydispersity has been incorporated into the block copolymer models, but most of them have been restricted to weak/strong segregation limits[34−36] or SCFT models[11,15,16] that mimic polydispersity through the use of binary mixtures of block copolymers having different lengths. Recently, Sides and Fredrickson proposed an efficient SCFT method to study the effect that polydispersity has on the bulk phase behavior of block copolymer melts.[37,38]

In this current investigation, in which we searched for the equilibrium microphases of polydisperse ABC linear triblock copolymer melts, we focused specifically on a model of ABC triblock copolymers in which two of the blocks of the chain (AB or BC or AC) are monodisperse and the polydispersity of the remaining block is characterized by a continuous molecular weight distribution. On the basis of these microphases, we constructed three-component triangle phase diagrams over the entire range of copolymer compositions having varied polydispersity for one particular block. This model and our results are particularly relevant to block copolymers produced by the new controlled free radical polymerization methods,[39,40] which are often much more "controlled" for one type of monomer than for another. Such studies are useful for understanding the mechanism through which one particular polydisperse block affects the formation of equilibrium microphases of ABC linear triblock copolymer melts. Our study extends the work[37,38] performed by the Fredrickson's group on the self-assembly of polydisperse AB diblock melts by applying it to polydisperse ABC linear triblock melts by using a real-space SCFT approach.

2. Theoretical Section

We consider a melt of n linear ABC triblock copolymers involved in a volume V and the volume fractions of copolymer chains are f_A, f_B, and f_C (where $f_C = 1 - f_A - f_B$), respectively. In the self-consistent mean-field theory, the free energy function (in units of k_BT) of the polydisperse system is given[37,38] by

$$F = -\int_0^\infty \mathrm{d}N'\Psi(N')\ln(Q_P/V) + \frac{1}{V}\int \mathrm{d}r[\chi_{AB}N_n\phi_A\phi_B + \chi_{AC}N_n\phi_A\phi_C + \chi_{BC}N_n\phi_B\phi_C - \omega_A\phi_A - \omega_B\phi_B - \omega_C\phi_C - P(1 - \phi_A - \phi_B - \phi_C)] \quad (1)$$

where N_n represents the number-average chain length; ϕ_A, ϕ_B, and ϕ_C are the monomer density fields normalized by the local volume fractions of A, B and C, respectively; ω_A, ω_B and ω_C are the conjugate fields; χ_{ij} is the Flory−Huggins interaction parameter between species i and j; P is the Lagrange multiplier (as a pressure); the partition function of a single-chain $Q_P = \int \mathrm{d}r q(r,N'/N_n)$ is an explicit functional of N' and is weighted by $\Psi(N')$, which is the probability density normalized for chain length.

The end-segment distribution function $q(r, s)$ gives the probability that the section of a chain, having contour length s and containing a free chain end, has its "connected end" located at r. It satisfies the modified diffusion equation

$$\frac{\partial}{\partial s}q(r, s) = R_{g0}^2\nabla^2 q(r, s) - \sum_I \gamma_I(s)\omega_I(r)q(r, s) \quad (I = \mathrm{A, B, C}) \quad (2)$$

where the lengths are scaled by R_{g0}, the (overall) radius of gyration of an unperturbed chain, and $\gamma_I(s)$ is 1 if s belongs to blocks I, and 0 otherwise. The appropriate initial condition is $q(r, 0) = 1$. Similarly, we need a second distribution function $q'(r, s)$ (containing the other chain end) that satisfies both $q'(r, N') = 1$ and eq 2 when the right-hand side is multiplied by -1.

In the preparation of block copolymers, polymerization of each monomer species along the chain may proceed through a distinct chemical process. Thus, perfect control over the molecular weight of every block is impossible for an ABC triblock copolymer. In this present study, we used an ideal model in which only the K block has variable chain length and the L and M blocks are treated as monodisperse [$(KLM) \in \{(\mathrm{ABC}),(\mathrm{BCA}),(\mathrm{CAB})\}$]. We chose a continuous molecular weight distribution function, the Schulz chain-length distribution $\Psi(N)$,[41] which is defined as $[(N_H)/N_h]^{\alpha-1}\exp[-(N_H)/N_h]/N_h\Gamma(\alpha)$ if H belongs to polydisperse block K and 0 otherwise, to be a realistic model of the polydisperse ABC blocks having an overall number-average $N_n = \alpha N + N_L + N_M$. The term α is determined from the equation $I_{\mathrm{pdi}}^K = (\alpha + 1)/\alpha$, the polydispersity index of the K block.

The mean-field SCF equations are obtained by using the saddle-point approximation, where one sets $\delta F/\delta\phi_i = \delta F/\delta P = \delta F/\delta\omega_i = 0$, which leads to the following set of equations:

$$\omega_A(r) = \chi_{AB}N_n(\phi_B(r) - f_B) + \chi_{CA}N_n(\phi_C(r) - f_C) + P(r) \quad (3)$$

$$\omega_B(r) = \chi_{AB}N_n(\phi_A(r) - f_A) + \chi_{BC}N_n(\phi_C(r) - f_C) + P(r) \quad (4)$$

$$\omega_C(r) = \chi_{CA}N_n(\phi_A(r) - f_A) + \chi_{BC}N_n(\phi_B(r) - f_B) + P(r) \quad (5)$$

$$\phi_A(r) + \phi_B(r) + \phi_C(r) = 1 \quad (6)$$

$$\phi_A(r) = \int_0^\infty \mathrm{d}N'\frac{\Psi(N')}{Q_P(N'/N_n)}\int_0^{N_A'/N_n}\mathrm{d}s q(r, s)q'(r, s) \quad (7)$$

$$\phi_B(r) = \int_0^\infty \mathrm{d}N'\frac{\Psi(N')}{Q_P(N'/N_n)}\int_{N_A'/N_n}^{(N_A' + N_B')/N_n}\mathrm{d}s q(r, s)q'(r, s) \quad (8)$$

$$\phi_C(r) = \int_0^\infty \mathrm{d}N'\frac{\Psi(N')}{Q_P(N'/N_n)}\int_{(N_A' + N_B')/N_n}^{N'/N_n}\mathrm{d}s q(r, s)q'(r, s) \quad (9)$$

Here, constant shifts in the potential are introduced in eqs 3−5; N_A', N_B', and $N_C' = N' - N_A' - N_B'$ are the chain lengths of the A, B, and C segments, respectively, on every chain. Note that eqs 7−9 are not available for a monodisperse triblock copolymer chain; they should be replaced by the eqs 7−9 presented in ref 24.

We solved eqs 3−9 directly in real space by using the combinatorial screening algorithm proposed by Drolet and Fredrickson.[29,30] This method involves a search for low free-energy solutions of the equations within a planar square or box having a periodic boundary condition. The relaxation scheme for calculating the saddle-point values for the fields was implemented through the following steps:

(1) Define a uniform grid within the simulation cell. Set the initial values of ω_A, ω_B, and ω_C at every point on the grid by using a random number generator.

(2) The modified diffusion equations are solved numerically by using a "pseudospectral method"[38,42] to calculate $q_g(r, s)$ and $q_g'(r, s)$ for each of the n_g terms.

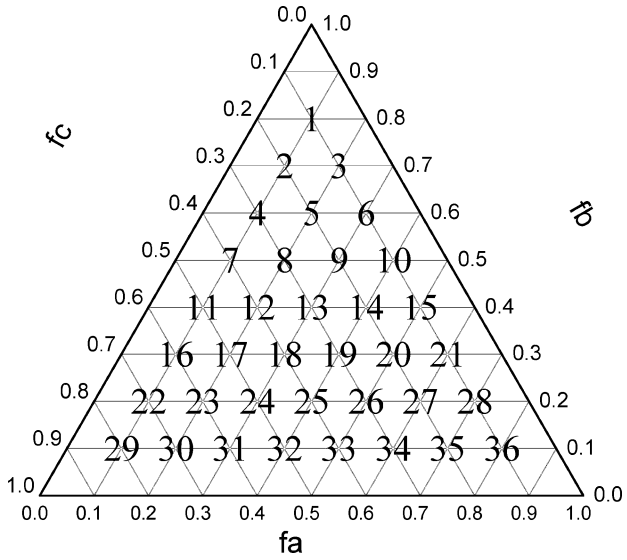

Figure 1. The locations within the phase diagram; nos. 1−36 correspond to the morphologies of the phases in Figures 2−6. The coordinates fa, fb, and fc represent the volume fractions of the A, B, and C blocks, respectively.

(3) An n_g-point Gaussian quadrature scheme[38,43] is adopted (e.g., $n_g = 4-8$ is sufficient for the results presented herein) to numerically evaluate the integrals of eqs 7−9.

(4) The chemical potential field ω_I can be updated by using the equation $\omega_I^{new} = \omega_I^{old} + \Delta t(\delta F/\delta\phi_I)^*$, where $(\delta F/\delta\phi_I)^* = \sum_{M\neq I}\chi_{IM}(\phi_M(r) - f_M) + P(r) - \omega_I^{old}$ is the chemical potential force.

(5) The effective pressure field, $P = C_2C_3(\omega_A + \omega_B) + C_1C_3(\omega_B + \omega_C) + C_1C_2(\omega_A + \omega_C)/2(C_1C_2 + C_2C_3 + C_1C_3)$, on each grid is obtained through solving eqs 3−6, where $C_1 = \chi_{CA} + \chi_{BC} - \chi_{AB}$, $C_2 = \chi_{CA} + \chi_{AB} - \chi_{BC}$, and $C_3 = \chi_{AB} + \chi_{BC} - \chi_{CA}$.

The numerical simulation was performed in the two-dimensional (2D) cell having periodic boundary conditions. Because the final morphologies can be influenced by the size of the simulation box,[32] two types of methods are used commonly to change the box size to minimize the free energy: (I) the cubic simulation cell shape is fixed and the cell size is adjusted[42] or (II) the cell size and shape are both adjusted.[24,44] In our simulation, we used the former method, i.e., $L_x = L_y$ is fixed and the size of the lattice spacing dx (and dy) was adjusted so that $\partial F(\mathrm{d}x_{min})/\partial(\mathrm{d}x) = 0$. The average chain length of the polymers was fixed at $N_n = 100$. In addition, to allow a comparison of the results obtained at different values of the polydispersity index I_{pdi}^K of the polydisperse block K, we adjusted the Schulz parameter N_k to maintain both the average monomer densities and $\chi_{ij}N_n$ constant. Noticeably, for the modified diffusion eq 1, the pseudospectral method provided a higher accuracy $(\Delta s)^3$ than did the Crank−Nicholson method[24] $(\Delta s)^2$, and Δs was 0.01 in the present system. Next, we performed the simulation for each sample until the phase pattern was stable, invariable with time, and $\Delta F < 10^{-6}$. Obviously, the results presented in this paper are subject to the 2D model and, hence, may not necessarily be applied to the solution of those intrinsic three-dimensional (3D) structures. The results obtained from the 2D model, however, have a large range of potential applications, including studies of nanolithographic

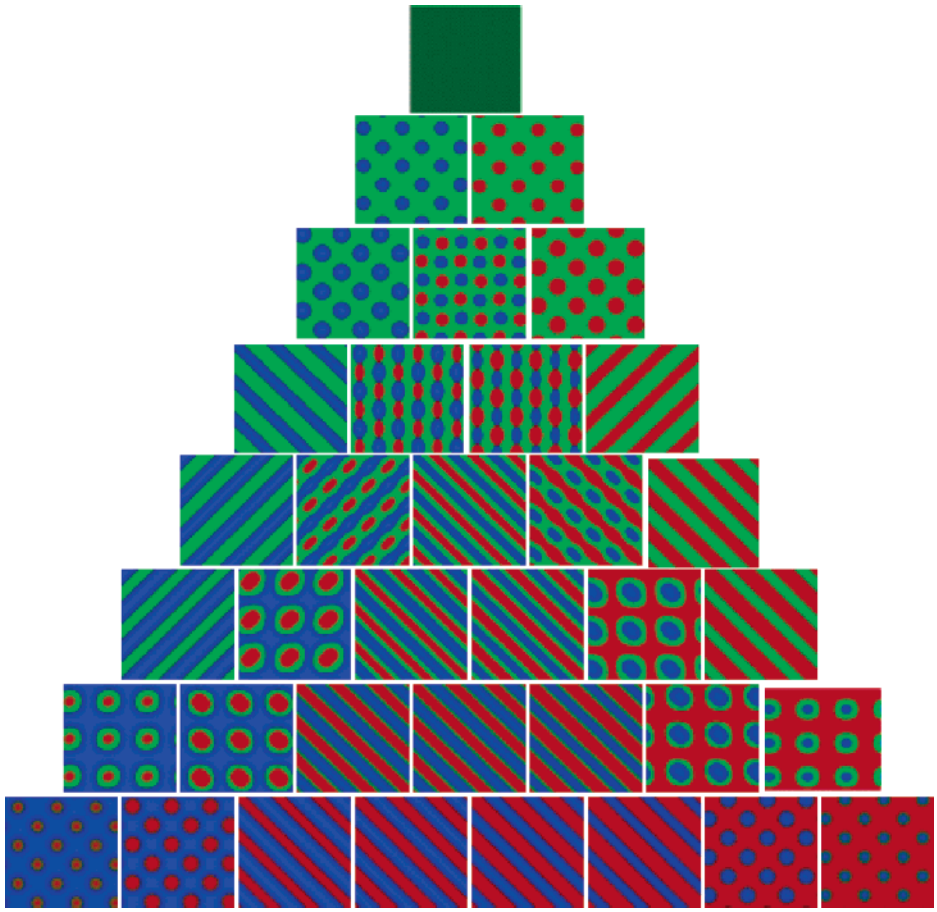

Figure 2. Phase diagram of monodisperse linear ABC triblock copolymers having binary interaction parameters $\chi_{AB}N_n = \chi_{BC}N_n = \chi_{AC}N_n = 35$. The red, green, and blue regions represent the density distributions of the monomers belonging to the A, B, and C blocks, respectively

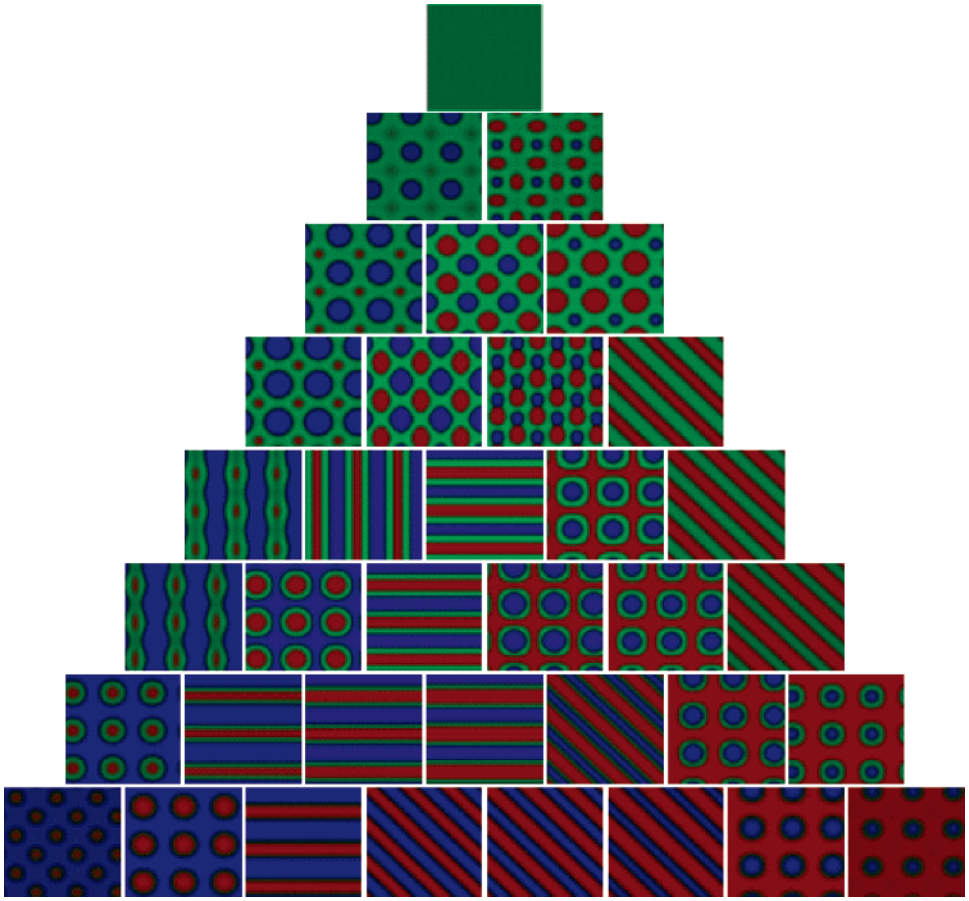

Figure 3. Phase diagram of linear ABC triblock copolymers exhibiting polydispersity in the C block at a polydispersity index of $I_{pdi}^{C} = 1.5$. The same interaction parameters are used as those described in Figure 2.

templates, membranes, and precursors for quantum electronic arrays. Moreover, even in a 3D system, microphases having translational invariance along certain directions, such as lamellar and cylindrical phases, can also be investigated by using a 2D model.

3. Results and Discussion

In the case of a diblock copolymer, the phase diagram can be depicted readily on a two-dimensional space because the microstructures are determined by two independent parameters. As stated in the Introduction, however, for an ABC triblock copolymer, the microstructures are determined by a total of five independent variables. It is difficult to depict all of the possible microstructures in a single phase diagram, but it is possible to draw a three-component triangle phase diagram (Figure 1) by observing the dependence of the microstructures on the components of the three blocks having invariant interaction energies between distinct blocks. Qiu and co-workers have depicted phase diagrams in this manner previously.[24] In our first attempt and for the sake of simplicity, we considered an ideal case in which the interaction energies between distinct blocks were all equal. The parameters in the calculation are assumed to be $N = 100$, $\chi_{AB}N = \chi_{BC}N = \chi_{AC}N = 35$, i.e., they are similar to those presented by Qiu and co-workers previously.[24] We observe, however, some differences between the phase diagrams obtained individually by our two groups. We attribute this result to the different methods that our groups used to change the size of the simulation box to minimize the free energy. In ref 24, the lattice spacings (i.e., dx and dy) and the lattice sizes (i.e., L_x and L_y) were changed. In our systemn, to obtain the lowest free energy, we maintained L_x to be equal to L_y and then changed the value of a (dx = dy = a) according to $\partial F(\mathrm{d}x_{min})/\partial(\mathrm{d}x) = 0$. Because the purpose of this study was to investigate the influence that the polydispersity has on the microstructures, we planned to begin with a well-studied monodisperse system so that our initial calculations could be compared with previous results. For convenience in our descriptions, we assigned a set of digital numbers on the grids in Figure 1; on each, the volume fraction of the monomers belonging to one of the three blocks can be calculated directly.

3.1. The Case of Monodisperse Triblock Copolymers. Figure 2 depicts the phase diagram of a monodisperse ABC triblock copolymer. The red, green, and blue regions represent the density distributions of the monomers belonging to the A, B, and C blocks, respectively. Because the A and C blocks are the two end blocks of the ABC triblock copolymer chain, the A and C components are symmetrical in this diagram about the line along which the B monomers have an equal volume fraction. For example, the patterns at nos. 12 and 14 are identical if we exchange the red (A component) and blue (C component) colors.

In comparison with the diblock copolymer, because of the increase in the number of independent parameters, we found, as expected, that the triblock copolymer system is characterized by more enriched microstructures. As Figure 2 indicates, even with an invariant interaction energy between the distinct blocks, the whole phase diagram can still be characterized by six typical microstructures: I, disordered phase (corresponding to no. 1 in Figure 1); II, interpenetrating tetragonal lattice (corresponding to nos. 2−6, 8, and 9 in Figure 1; the domains of the minority

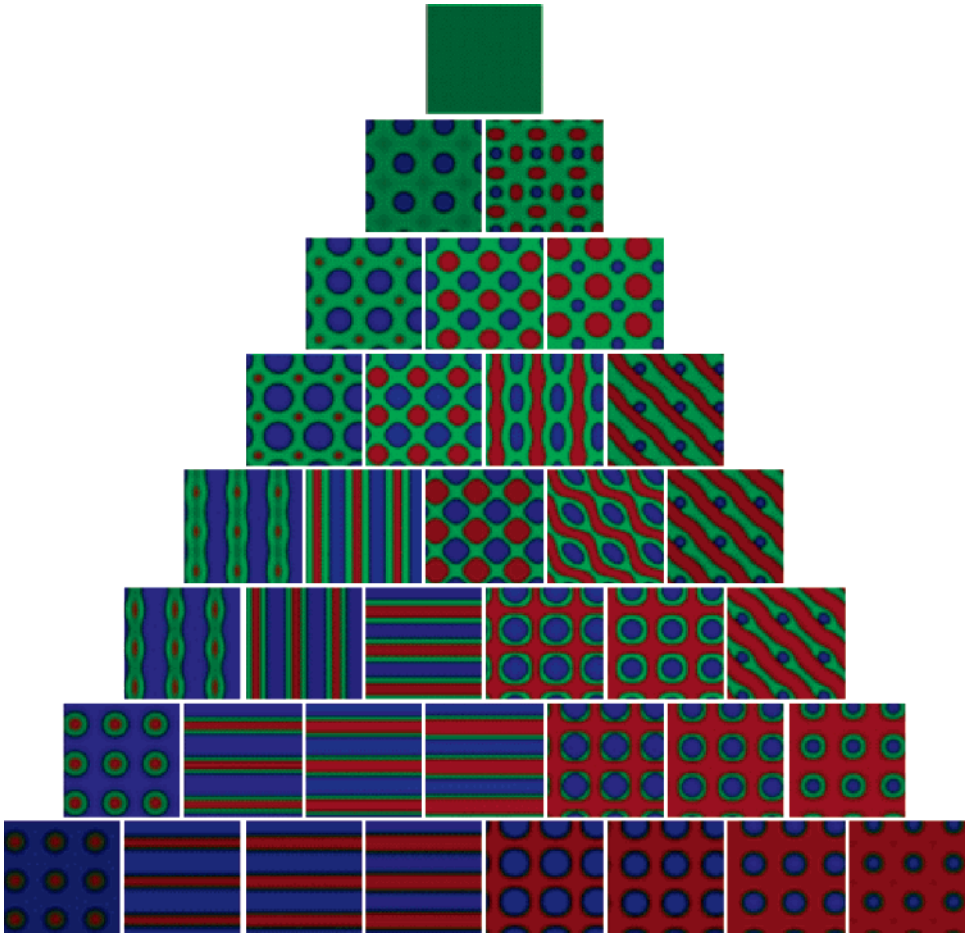

Figure 4. Phase diagram of linear ABC triblock copolymers exhibiting polydispersity in the C block at a polydispersity index of $I_{pdi}^{C} = 2.0$. The same interaction parameters are used as those described in Figure 2.

components, red in nos. 2 and 4 and blue in nos. 3 and 6, are not obvious); III, two-color lamellae (nos. 7, 10, 11, 15, 16, 21, 31−34); IV, three-color lamellae (nos. 13, 18, 19, 24−26); V, core/shell tetragonal lattice (nos. 17, 20, 22, 23, 27−30, 35, 36); VI, lamellar phase with beads inside (nos. 12 and 14).

We determined the interaction energies between two distinct blocks to ensure the incompatibility between any of the two components. Thus, the microstructures should depend on both the volume fraction of each component and the architecture of the triblock copolymer chain. For an ABC linear triblock copolymer chain, the microstructures should be arranged in the manner in which the B phase exists between the A and C phases to avoid their connection. On the basis of this point of view, we can understand the phase diagram in Figure 2. When the A and C blocks are very short, <10% in volume fraction, the A and C phases are invisible because of their low concentrations, which leads to the disordered phase presented at position no. 1 in Figure 2. When the fraction of monomers belonging to the B block is in the majority, the dispersed A and C phases are embedded in the matrix comprising the monomers belonging to the B block and form a microphase of type II. If one of the three blocks is too short, while the other two blocks are comparable in length, the architecture of the triblock copolymer chain is similar to that of a symmetrical diblock copolymer chain, and as expected, typical two-color lamellae (type III) are obtained as a result. If the three blocks are comparable in length, the patterns are formed from the manner in which the B phase resides between the A and C phases to separate these two phases as far apart as possible because the B block is in the middle of the triblock copolymer chain. Pattern no. 13 on the grid, corresponding to the most symmetrical triblock copolymer having respective length fractions of blocks A, B, and C of 0.30, 0.40, and 0.30, respectively, is typical of the three-color lamellas (type IV) having the B phase (green) residing at the interfaces between the A and C phases. When one of the two end blocks, A or C, becomes shorter, the A phase (or C phase) cannot form uniform lamella. Instead, to avoid the connection between the A and C phases, they are embedded in the lamellas formed by the B phase, leading to the formation of phases of type VI at nos. 12 and 14. Upon further decreases in the faction of the B block, the B block becomes too short to form continuous lamellar patterns; instead, core/shell patterns form, as indicated in nos. 17, 20, 22, 23, 27−30, 35, and 36, in which the B phase forms the shells to avoid connection between the A and C phases. In cases, however, where the A and C blocks are comparable in length and long enough, the A and C blocks prefer to form the lamellas, and thus, the B block is forced to reside at the interfaces between the A and C phases and forms three lamellas, as on grid nos. 18, 19, and 24−26.

3.2. The Case of a Polydisperse End Block. First, we considered the case in which the A and B blocks were of fixed length and the C block was polydisperse. The molecular parameters, the polymerization index N_n, and the Flory−Huggins interaction parameters between the distinct species χ_{AB}, χ_{BC}, and χ_{AC} were chosen to be identical with those described above for the case of the monodisperse copolymers, and thus, any variations in the microstructures are guaranteed to arise solely

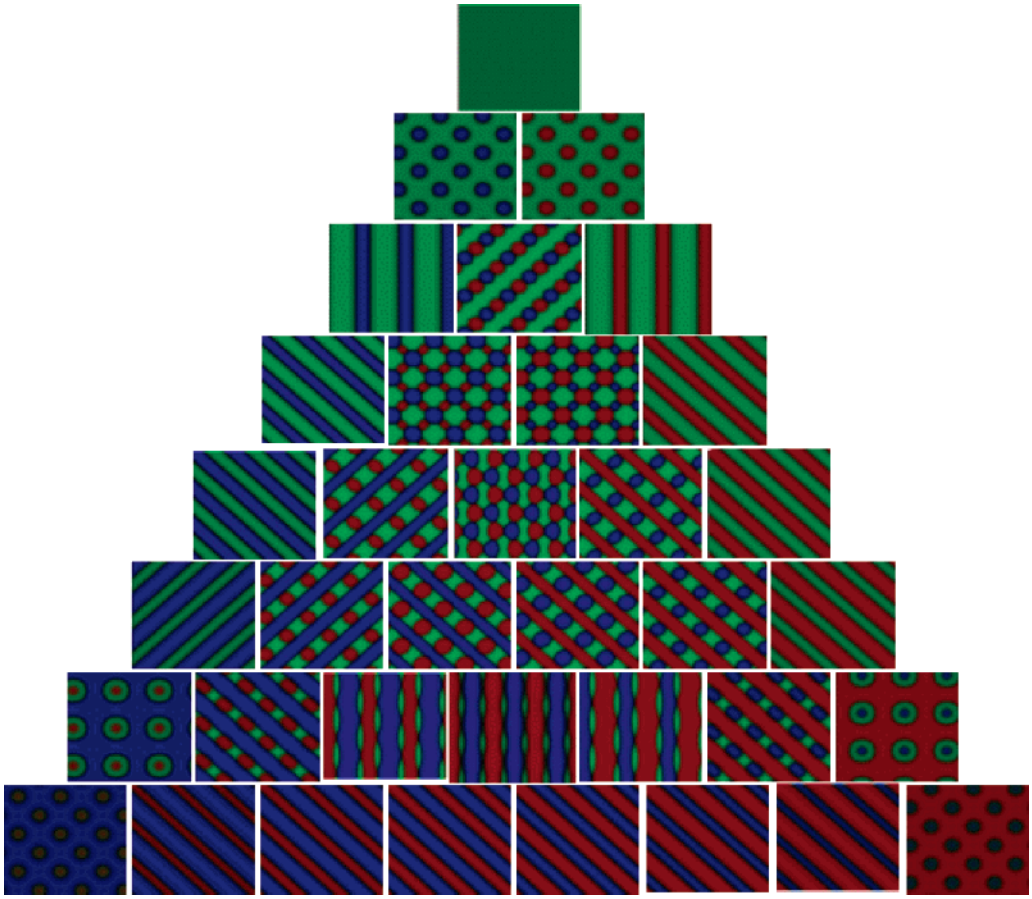

Figure 5. Phase diagram of linear ABC triblock copolymers exhibiting polydispersity in the B block at a polydispersity index of $I^{B}_{pdi} = 1.5$. The same interaction parameters are used as those described in Figure 2.

from the polydispersity of the C block. Figure 3 displays the diagram of the polydisperse ABC triblock copolymers at $I^{C}_{pdi} = 1.5$. There are six typical patterns present in Figure 3: I, disordered phase at no. 1; II, interpenetrating tetragonal lattice at nos. 2−9; III, two-color lamellas at nos. 10, 15, 21, and 32−34; IV, three-color lamellas at nos. 12, 13, 18, 23−26, and 31; V, core/shell tetragonal lattices at nos. 14, 17, 19, 20, 22, 27−30, 35, and 36; VI, lamellar phases with beads inside at nos. 11 and 16. Figure 4 displays the diagram obtained at $I^{C}_{pdi} = 2.0$. There are seven typical patterns: I, disordered phase at no. 1; II, interpenetrating tetragonal lattices at nos. 2−8 and 13; III, two-color lamellas at nos. 30−32; IV, three-color lamellas at nos. 12, 17, 18, and 23−25; V, core/shell tetragonal lattices at nos. 19, 20, 22, 26−29, and 33−36; VI, lamellar phases with beads inside at nos. 9, 11, 14 and 16; VII, lamellar phases with beads on the surface at nos. 10, 15, and 21.

As we noted for the patterns at nos. 2−4 and 6 in Figure 2, the minority components, i.e., A monomers (red color) at nos. 2 and 4 or C monomers (blue color) at nos. 3 and 6, are not explicitly observable. In contrast, these minority components are clearly visible at nos. 3, 4, and 6 in Figures 3 and 4; this situation indicates that the polydisperse C blocks may drive the strong segregation among these three blocks. Moreover, the invisible red domain on the pattern at no. 2 and the visible blue domain on the pattern at no. 3 in Figures 3 and 4 demonstrate that the C block is relatively easily segregated in comparison with the A block. This conclusion is further verified in Figures 3 and 4 by the fact that the domain (red) comprised of A blocks at no. 4 is smaller in size than that (blue) comprising C blocks at no. 6. In addition, we observe that all of the dispersed domains at nos. 2−5 in Figures 3 and 4 are larger in size than those in Figure 2. Fredrickson has also observed that larger domain sizes resulted from dispersed blocks in diblock copolymer systems.[38] In summary, the patterns influenced by the polydispersity of the C block can be characterized by two features: it induces strong segregation among the three components and it causes the dispersed domain to become larger in size. The difference between the patterns of the monodisperse ABC triblock copolymer in Figure 2 and those of the polydisperse ones in Figures 3 and 4 can be understood in terms of these two phenomena. For example, the two-color lamellas at nos. 11 and 16 in Figure 2 are transferred into the pattern of lamellas with beads inside in Figures 3 and 4 because the polydisperse C blocks drive the segregation of A blocks from the domain comprising the mixture of A and B components; in fact, the green lamellas at nos. 11 and 16 in Figure 2 comprise a mixture of the A and B components. For the same reason, upon increasing the polydispersity of the C block, the two-color lamellas at nos. 10, 15, and 21 in Figures 2 and 3 are transferred into the lamellas with beads on their surface in Figure 4. In a second example, which is due to the tendency to form larger domain sizes at larger polydispersities of the C block I^{C}_{pdi}, the patterns of the lamellas with beads inside at no. 14 in Figure 2 convert to the core/shell tetragonal lattices in Figure 3 because the geometric volume of the B component is so small that it is not large enough to form lamellas having a large domain of C blocks embedded within them. Thus, the core/shell structures are formed to minimize the free energy of the system. Upon a further increase, however, in the size of the dispersed phase of the C block (the blue one) that occurs upon increasing the polydispersity of the C block, the outside surfaces of two closed shells comprising B blocks can touch, which, again, results in

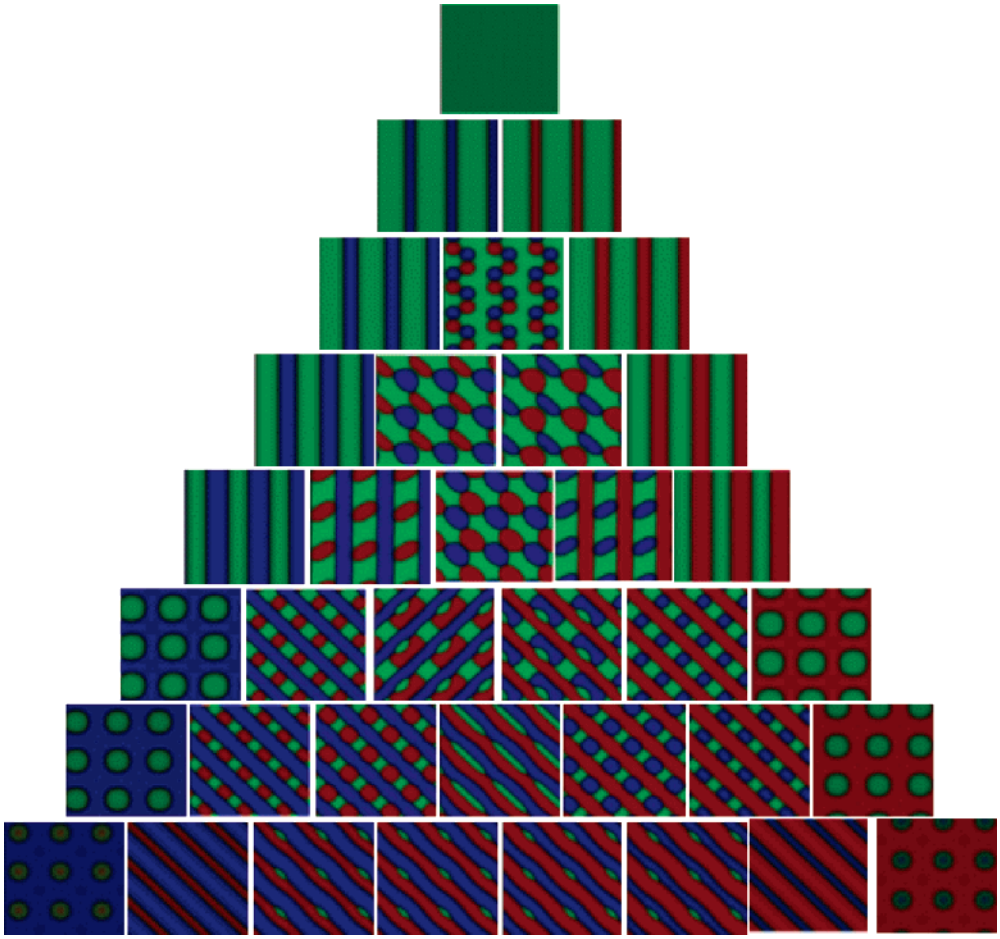

Figure 6. Phase diagram of linear ABC triblock copolymers exhibiting polydispersity in the B block at a polydispersity index of $I_{pdi}^{B} = 2.0$. The same interaction parameters are used as those described in Figure 2.

the formation of lamellas with beads inside, as depicted at no. 14 in Figure 4.

3.3. The Case of a Polydisperse Middle Block. In this subsection we consider cases in which the middle block (B block) is polydisperse and the two end blocks (A and C) have fixed lengths. There are nine typical patterns in the diagram presented in Figure 5 for the case of $I_{pdi}^{B} = 1.5$. They are: I, disordered phase at no. 1; II, tetragonal lattices at nos. 2 and 3; III, two-color lamellas at nos. 4, 6, 7, 10, 11, 15, 16, 21, and 30−35; IV, core/shell tetragonal lattices at nos. 22, 28, 29, and 36; V, lamellas with alternative beads at no. 5; VI, three-color interpenetrating tetragonal lattices at nos. 8 and 9; VII, bamboo-like lamellas at nos. 12, 14, 17−20, 23, and 27, VIII, lamellas having beads on the surface at nos. 24−26; IX, alternative diamonds at no. 13. There are seven typical patterns in the diagram presented in Figure 6 for case $I_{pdi}^{B} = 2.0$. They are: I, disordered phase at no. 1; II, two-color lamellas at nos. 2−4, 6, 7, 10, 11, 15, 30, and 35; III, wavelike alternative-bead lamellas at no. 5; IV, alternative diamonds at nos. 8, 9, and 13, V, bamboo-like lamellas at nos. 12, 14, 17, 20, 23, 24, 26, and 27; VI, boatlike lamellas at nos. 18 and 19; VII, lamellas having beads on the surface at nos. 25 and 31−34.

A distinct feature in Figures 5 and 6 that is very different from the case of the homodisperse ABC triblock copolymer in Figure 2 is that the phases comprising B components have a tendency not to reside on the interfaces between the A and C phases. Most of the patterns are characterized by the manner of the connection between the A (red) and C (blue) phases. To understand the influence of the polydispersity of the B block, Figure 7 displays the density distributions contributed by polymers having different chain lengths on the pattern at no. 22 in Figure 6, parametrized by different Gaussian quadratures ($n_g = 6$) having a larger value of g, which corresponds to a longer chain. Figure 7A indicates that, in the case of monodisperse triblock copolymers, the major part of the A component is concentrated in the central area, whereas the B component is distributed as a shell around it to form a core/shell structure. At a low polydispersity of the B block ($I_{pdi}^{B} = 1.5$), the type of density distribution is similar to that of monodisperse triblock copolymers (Figure 7B), but at a high polydispersity (e.g., $I_{pdi}^{B} = 2.0$), both the A and B components are almost homogeneously distributed in the domain, as indicated in Figure 7C1. This situation arises because the longer chains [corresponding to larger values of g (3 or 4)] have a tendency to self-aggregate at the central area of the domain. In our calculations, we used an average chain length of 100 monomers. For the chains at no. 22 in Figure 6, we fixed the number of monomers in the A and C blocks at 10 and 70, respectively; the average number of monomers in block B was 20. In the case when $I_{pdi}^{B} = 2.0$, the corresponding lengths of the B block for $g = 1$, 2, 3, and 4 were 6, 18, 39, and 70 monomers, respectively. Because of the longer block B and the shorter block A (10 monomers) when g was either 3 or 4, these triblock copolymer chains have characteristics that are more like those of a diblock copolymer. As a result, the B block itself forms a dispersed phase, i.e., it is concentrated at the central area of the domain, as indicated in Figure 7C3. Furthermore, the A blocks that occupy the central region in Figure 7A have been repelled to the outside. Our

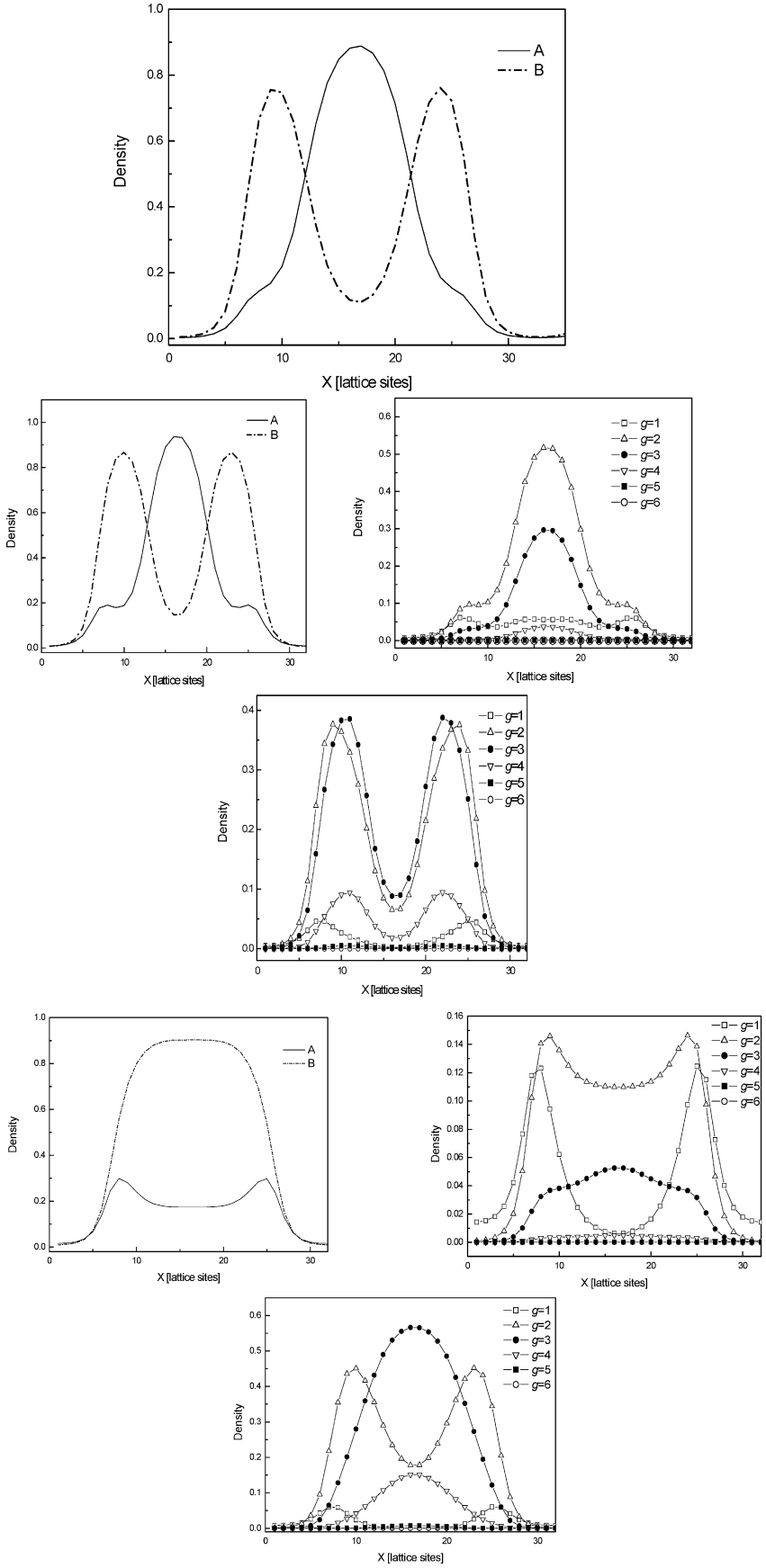

Figure 7. Density distributions of A and B monomers having different chain lengths. (A) Density distributions of A and B blocks at no. 22 in Figure 2 (i.e., monodisperse linear ABC block copolymer); (B1) density distributions of A and B blocks at no. 22 in Figure 5 (i.e., polydispersity index $I_{\mathrm{pdi}}^{\mathrm{B}} = 1.5$); (B2) density distributions of A monomers having different B chain lengths; (B3) density distributions of B monomers having different chain lengths; (C1) density distributions of A and B blocks at no. 22 in Figure 6 (i.e., polydispersity index $I_{\mathrm{pdi}}^{\mathrm{B}} = 2.0$); (C2) density distributions of A monomers having different B chain lengths; (C3) density distributions of B monomers having different chain lengths.

analysis reveals that when the B blocks have larger polydispersity, longer B blocks tend to self-aggregate rather than reside at the interface, and this phenomenon results in the phase patterns presented in Figures 5 and 6.

4. Conclusion

By using a 2D real-space self-consistent field theory, we have depicted, by using a three-component triangle style, the phase diagrams of monodisperse ABC triblock copolymers having fixed interaction energies between their distinct blocks. Next, we studied the influence that the polydispersity of the end and middle blocks has on the microstructures. We modeled the molecular weight distribution using the Schulz distribution, which is a continuous chain-length distribution that is amenable to analytical and numerical analysis. Our simulation indicated that polydisperse end blocks (A or C blocks) lead to strong segregation among the three components and to larger domain sizes of dispersed phases. On the other hand, a polydisperse middle block (B block) leads to a connection between the phases formed by the two end blocks. This analytical approach allows us to understand the changes that occur to the microstructures in the phase diagram as a consequence of the presence of the polydisperse blocks.

Acknowledgment. This research was supported by the General Program (203074050, 90403022) and the Major Program (20490220) of the National Natural Science Foundation of China (NSFC), the 973 Program of MOST (no. 2005CB-623807) A.C.S. acknowledges the support of the Natural Science and Engineering Research Council (NSERC) of Canada and the Research Corporation.

References and Notes

(1) Hamley, I. W. *The Physics of Block Copolymers*; Oxford University Press: New York, 1998.
(2) Khandpur, A. K.; Foster, S.; Bates, F. S.; Hamley, I. W.; Ryan, A. J.; Almdal, K.; Mortensen, K. *Macromolecules* **1995**, *28*, 8796.
(3) Matsen, M. W.; Bates, F. S. *Macromolecules* **1996**, *29*, 1091; Matsen, M. W.; Bates, F. S. *J. Chem. Phys.* **1997**, *106*, 2436.
(4) Matsen, M. W. *J. Chem. Phys.* **2000**, *113*, 5539.
(5) Tyler, C. A.; Morse, D. C. *Phys. Rev. Lett.* **2005**, *94*, 208302.
(6) Winey, K. I.; Thomas, E. L.; Fetters, L. J. *Macromolecules* **1992**, *25*, 2645.
(7) Hadjuk, D. A.; Harper, P. E.; Gruner, S. M.; Honecker, C. C.; Kim, G.; Thomas, E. L.; Fetters, L. J. *Macromolecules* **1994**, *27*, 4063.
(8) Hashimoto, T.; Yamasaki, K.; Koizumi, S.; Hasegawa, H. *Macromolecules* **1993**, *26*, 2895.
(9) Zhao, J.; Majumdar, B.; Schulz, M. F.; Bates, F. S.; Almdal, K.; Mortensen, K.; Hajduk, D. A.; Gruner, S. M. *Macromolecules* **1996**, *29*, 1204.
(10) Lai, C.; Russel, W. B.; Register, R. A.; Marchand, G. R.; Adamson, D. H. *Macromolecules* **2000**, *33*, 3461.
(11) Matsen, M. W. *Macromolecules* **1995**, *28*, 5765.
(12) Whitmore, M. D.; Noolandi, J. *Macromolecules* **1985**, *18*, 2486.
(13) Lyatskaya, Yu. V.; Zhulina, E. B.; Birshtein, T. M. *Polymer* **1992**, *33*, 343.
(14) Spontak, R. J. *Macromolecules* **1994**, *27*, 6363.
(15) Matsen, M. W.; Bates, F. S. *Macromolecules* **1995**, *28*, 7298.
(16) Matsen, M. W. *Phys. Rev. Lett.* **1995**, *74*, 4225.
(17) Mogi, Y.; Mori, K.; Matsushita, Y.; Noda, I. *Macromolecules* **1992**, *25*, 5412.
(18) Stadler, R.; Auschra, C.; Beckmann, J.; Krappe, U.; Voigtmartin, L.; Leibler, L. *Macromolecules* **1995**, *28*, 3080.
(19) Breiner, U.; Krappe, U.; Thomas, E. L.; Stadler, R. *Macromolecules* **1998**, *31*, 135.
(20) Goldacker, T.; Abetz, V. *Macromolecules* **1999**, *32*, 5165.
(21) Mogi, Y.; Kotsuji, H.; Kaneko, Y.; Mori, K.; Matsushita, Y.; Noda, I. *Macromolecules* **1992**, *25*, 5408.
(22) Zheng, W.; Wang, Z.-G. *Macromolecules* **1995**, *28*, 7215.
(23) Gido, S. P.; Schwark, D. W.; Thomas, E. L.; Goncalves, M. *Macromolecules* **1993**, *26*, 2636.
(24) Tang, P.; Qiu, F.; Zhang, H. D.; Yang, Y. L. *Phys. Rev. E* **2004**, *69*, 031803.
(25) Edwards, S. F. *Proc. Phys. Soc.* **1965**, *85*, 613.
(26) Helfand, E. *J. Chem. Phys.* **1975**, *62*, 999.
(27) Matsen, M. W.; Schick, M. *Phys. Rev. Lett.* **1994**, *72*, 2660.
(28) Noolandi, J.; Shi, A.-C.; Linse, P. *Macromolecules* **1996**, *29*, 5907.
(29) Drolet, F.; Fredrickson, G. H. *Phys. Rev. Lett.* **1999**, *83*, 4317.
(30) Drolet, F.; Fredrickson, G. H. *Macromolecules* **2001**, *34*, 5317.
(31) Fredrickson, G. H.; Ganesan, V.; Drolet, F. *Macromolecules* **2002**, *35*, 16.
(32) Bohbot-Raviv, Y.; Wang, Z.-G.; *Phys. Rev. Lett.* **2000**, *85*, 3428.
(33) Jian, T.; Anastasiadis, S. H.; Semenov, A. N.; Fytas, G. *Macromolecules* **1995**, *28*, 2439.
(34) Dobrynin, A. V. *Macromolecules* **1997**, *30*, 4756.
(35) Milner, S. T.; Witten, T. A.; Cates, M. E. *Macromolecules* **1989**, *22*, 853.
(36) Pagonabarraga, I.; Cates, M. E. *Europhys. Lett.* **2001**, *55*, 348.
(37) Fredrickson, G. H.; Sides, S. W. *Macromolecules* **2003**, *36*, 5415.
(38) Sides, S. W.; Fredrickson, G. H. *J. Chem. Phys.* **2004**, *121*, 4974.
(39) Chong, B. Y. K.; Le, T. P. T.; Moad, G.; Rizzardo, E.; Thang, S. H. *Macromolecules* **1999**, *32*, 2071.
(40) Bendejacq, D.; Ponsinet, V.; Joanicot, M.; Loo, Y. L.; Register, R. A. *Macromolecules* **2002**, *35*, 6645.
(41) Schulz, G. V. Z. *Z. Phys. Chem. (Munich)* **1939**, *B43*, 25.
(42) Sides, S. W.; Fredrickson, G. H, *Polymer* **2003**, *44*, 5859.
(43) Press, W. H.; Teukolsky, S. A.; Vetterling, W. T.; Flannery, B. P. *Numerical Recipes in C: The Art of Scientific Computing*, 2nd ed.; Cambridge University Press: Boston, 1992.
(44) Tyler, C. A.; Morse, D. C. *Macromolecules* **2003**, *36*, 8184.